Biointerface Research in Applied Chemistry
Open-Access Journal (ISSN: 2069-5837)

Article
Volume 15, Issue 1, 2025, 7
https://doi.org/10.33263/BRIAC151.007

Soret and Chemical Reaction Effects on MHD Convection-Free Flow Past a Suddenly Started Inclined Vertical Plate with Ramped Velocity, Temperature, and Concentration

Hiren Deka [1], Nazibuddin Ahmed [1], Puja Haloi [1,*]

[1] Department of Mathematics, Cotton University, Panbazar, Guwahati-781001, Assam, India: hiren.deka@cottonuniversity.ac.in (H.D); nazib@gauhati.ac.in (N.A.); pujahaloi2020@gmail.com (P.H);
* Correspondence: pujahaloi2020@gmail.com;

Scopus Author ID 55063915300

Received: 15.09.2024; Accepted: 2.01.2025; Published: 12.02.2025

Abstract: The combined impacts of thermal diffusion and thermal radiation on convection-free MHD heat-absorbing chemically reactive flow past an impulsively initiated inclined upright plate incorporating ramped velocity, ramped concentration, and ramped temperature are analyzed. This study presents a comparative assessment for both ramped and isothermal conditions. Leveraging the Heaviside step function, the unitless domain equations are tackled by implementing the Laplace transform technique. The influences of diverse embedded parameters on temperature, velocity, and concentration fields, as well as the momentum, mass, and heat transport rates, have been represented graphically and interpreted physically. Graphs are created with the help of MATLAB computing software. It is emphasized that an improved chemical reaction parameter lowers both velocity and concentration while simultaneously increasing the mass transport rate. Furthermore, an increase in the Soret effect enhances fluid velocity and concentration, showcasing a divergent behavior in mass transfer rate. Our analysis also reveals an intriguing finding: under both ramped and isothermal conditions, the ramped parameter escalates the fluid velocity near the plate; however, after a critical point, the trend reverses. This research holds substantial importance across various engineering fields, such as materials manufacturing, turbine heat transfer, and electronic circuit operations.

Keywords: Soret effect; chemical reaction; ramped parameter; inclined plate; thermal radiation.

Nomenclature: $\vec{B}$ magnetic flux density; C, molar species concentration (kmol/m^3); B_0 applied magnetic field strength (Weber/ m^2); C_p specific heat (J/kgK); C_s concentration susceptibility ({k(mol)^{2}s^2/m^8}; C_∞ free stream concentration (kmol/m^3); C_W plate concentration (kmol/m^3); D_M mass diffusivity (m^2/s); K_T thermal diffusion ratio; $\vec{q}$ fluid velocity vector; g, acceleration due to gravity (m^2/s); Sr Soret number; κ thermal conductivity (W/mK); Gr, thermal Grashof number; ρ_∞ fluid density outside the plate (kg/m^3); J, heat absorption parameter; Gm, solutal Grashof number; $\bar{J}$ heat sink (W/m^{3}K); $\bar{K}$ chemical reaction rate (s^{-1}); Ra ramped parameter; T_m mean fluid temperature (K); K chemical reaction parameter; N radiation parameter; $\vec{J}$ current density vector; M magnetic parameter; p, pressure (N/m^2); Sc Schmidt number; T temperature (K); q_r radiation heat flux (W/m^2); Pr Prandtl number; q^* heat flux (W/m^2); $\bar{t}$ time (s); T_W isothermal temperature for $\bar{t} > t_0$, (K); t_0 characteristic time (s); U_0 plate velocity; $\acute{u}$velocity component along X-axis (m/s); T_∞ undisturbed temperature (K); σ electrical conductivity (l/Ωm); ρ fluid density (kg/m^3); σ^* Stefan- Boltzmann constant (W/m^{2}K^4); ρ_∞ fluid density outside the plate (kg/m^3); κ^* mean absorption coefficient (l/m); β coefficient of thermal expansion (J/kgK); μ coefficient of viscosity (kg/ms); β^* coefficient of solutal expansion (l/kmol).

1. Introduction

In recent decades, extensive research into the coupled effects of heat and mass transport on convection-free hydromagnetic flow has gained widespread interest due to its predominant role in science, engineering, and industrial disciplines. It is found in petroleum technology, chemical and agricultural engineering, and several other disciplines. Within this remarkable extensive research, certain studies stand out as particularly impactful. They are Veera Krishna [1], Kataria and Patel [2], Roy [3], Kumar *et al*. [4], Anwar *et al*. [5], Karmakar *et al*. [6], and so on. Recently, Dowerah *et al*. [7] systematically examined the MHD natural convective flow past an impulsively started infinite upright plate, incorporating thermal radiation, chemical reaction, and radiation absorption. Das *et al*. [8] investigated the heat-mass transmission mechanism of an electrically low-performing hybrid nanofluid (rGO-magnetite-water) near a vertically straightened Riga plate sensor with ramped temperature and concentration.

Chemical reactions are integral to chemical engineering mechanisms, particularly in managing diverse heat and mass transport issues. The classification of chemical reactions into heterogeneous and homogeneous processes depends on whether they happen at an interface or within a single-phase volume. A chemical reaction involving a foreign mass and a fluid is a common occurrence in chemical engineering processes. Such processes are widely applied in polymer fabrication, food preparation, ceramics and glass crafting, and other similar industries. An elaborate assessment of this effect was undertaken by Sedki [9], Verma [10], Saikia and Ahmed [11], Kataria and Patel [12], Ibrahim and Suneetha [13], and Ali *et al*. [14]. In the presence of thermal radiation and chemical reaction, Das *et al*. [15] investigated the impact of slip condition and rotation on an unsteady MHD Darcy flow of a non-Newtonian Casson nanofluid past an infinite oscillating vertical plate with ramped temperature and concentration. The dynamics of a chemically reactive tri-hybridized nanofluid over a suddenly started vertical plate with ramped motion was studied by Ali *et al*. [16]. The study conducted by Ali *et al*. [17] analyzed an unsteady rotating MHD Darcy flow of a non-Newtonian hybrid nanofluid past an exponentially accelerated vertical plate under the influence of chemical reaction, velocity slip, Hall, and ion slip effects.

The Soret effect describes the mechanism through which a thermal gradient causes mass flux. Even though the Soret effect is not as influential as the effect governed by Fick's law, it is frequently ignored in several investigations. Nonetheless, there are numerous situations where exceptions are permitted. The Soret effect is vital and inescapable in many cases, as highlighted by Eckert and Drake [18]. In light of the significant role of the Soret effect, several comprehensive surveys have been executed by Mopuri *et al*. [19], Raghunath [20], Agrawal and Panda [21], Goud and Reddy [22], etc. Recently, Gohain *et al*. [23] explored MHD free convective flow past an upright plate, including ramped velocity and concentration under the impact of the Soret effect.

An object emitting electromagnetic waves as a consequence of its temperature is known as thermal radiation. Thermal radiation is released by all objects possessing a temperature higher than absolute zero (-273.15°C or 0K). Various industrial processes, such as space missions, archaeology, aeronautics, power production, and astrophysics, utilize radioactive flows. Research initiatives such as Endalew and Nayak [24], Ullah *et al*. [25], Das *et al*. [26], Yedhiri *et al*. [27], Ahmmed *et al*. [28], Ali *et al*. [29] examined various dimensions of the thermal radiation effect. Patel has inspected the impact of radiation on the MHD flow of micropolar fluid between two upright walls [30]. Ali *et al*. [31] explored the influence of thermal radiation on the MHD gyrating stream of a non-Newtonian modified hybrid nanofluid past a vertical plate with ramped motion, Newtonian heating, and Hall currents. Das *et al*. [32] conducted a research investigation to analyze the effects of thermal radiation and heat generation on MHD non-Newtonian fluid flow with ramped movement.

The principal focus of this ongoing study is to explore the impacts of the Soret effect, radiation, chemical reaction, and heat sink on the convection-free MHD flow past a suddenly started inclined upright plate. Based on the author's assessment, no existing studies delve into the concurrent implementation of ramped velocity, ramped plate temperature, and ramped concentration on MHD flow past an impulsively initiated inclined upright plate. The incorporation of thermal diffusion, thermal radiation, chemical reaction, and heat-absorbing effects on MHD free convective flow past an impulsively initiated inclined vertical plate, along with the simultaneous implementation of ramped conditions, sets our manuscript apart from previously proposed models, highlighting the novelty of our investigation.

2. Basic Equations with Assumptions

2.1. Basic equations.

The computational model that simulates the time-independent, viscous, incompressible MHD convective flow of chemically reactive fluid with radiation and heat absorption is:

Continuity equation (Das *et al*. [26]):

$$\vec{\nabla}.\vec{q}=0. \tag{1}$$

Gauss's law in magnetostatics (Das *et al*. [26]):

$$\vec{\nabla}.\vec{B}=0. \tag{2}$$

Electric current density (Das *et al*. [26]):

$$\vec{J}=\sigma(\vec{E}+\vec{q}\times\vec{B}). \tag{3}$$

Momentum equation (Das *et al*. [26]):

$$\rho\left[\frac{\partial\vec{q}}{\partial t}+\left(\vec{q}.\vec{\nabla}\right)\vec{q}\right]=-\vec{\nabla}p+\vec{J}\times\vec{B}+\rho\vec{g}+\mu\nabla^2\vec{q}. \tag{4}$$

Energy equation (Das *et al*. [26]):

$$\rho C_p\left[\frac{\partial T}{\partial t}+\left(\vec{q}.\vec{\nabla}\right)T\right]=\kappa\nabla^2 T+\bar{J}\left(T_\infty-T\right)-\vec{\nabla}.\vec{q}_r. \tag{5}$$

Species continuity equation (Das *et al*. [26]):

$$\frac{\partial C}{\partial t}+\left(\vec{q}.\vec{\nabla}\right)C=D_M\nabla^2 C+\bar{K}\left(C_\infty-C\right)+\frac{D_M K_T}{T_m}\nabla^2 T. \tag{6}$$

Equation of state:

$$\rho_\infty=\rho\left[1+\beta\left(T-T_\infty\right)+\beta^*\left(C-C_\infty\right)\right]. \tag{7}$$

As estimated by Das *et al*. [26], the radiative heat flux $\vec{q}_r$ is as follows:

$$\vec{q}_r=-\frac{4\sigma^*}{3\kappa^*}\vec{\nabla}T^4 \tag{8}$$

As per the assumption, the temperature variation stays minimal across the fluid flow. This allows us to represent T^4 as :

$$T^4=\left[T_\infty+(T-T_\infty)\right]^4\approx 4T_\infty^{\;3}T-3T_\infty^{\;4}. \tag{9}$$

By applying equations (8) and (9), equation (5) is simplified as:

$$\rho C_p\left[\frac{\partial T}{\partial \bar{t}}+\left(\vec{q}.\vec{\nabla}\right)T\right]=\kappa\nabla^2 T+\bar{J}\left(T_\infty-T\right)+\frac{16\sigma^* T_\infty^{\ 3}}{3\kappa^*}\nabla^2 T. \qquad (10)$$

Symbol specifications are outlined in the nomenclature section.

2.2. Basic assumptions.

The following key assumption guides our analysis:

- All fluid properties are maintained as constants, except for density in the buoyancy term.
- With a low magnetic Reynolds number assumption, the induced magnetic field is excluded from our analysis.
- External electric field effects are disregarded.
- The plate is electrically insulated.
- $T_w > T_\infty$ & $C_w > C_\infty$.

3. Problem Formulation

The cartesian coordinate system is positioned in such a way that the $\acute{x}$-axis is angling straight upwards, which is inclined at an angle γ with the vertical, the $\acute{y}$-axis is normal to the plate, and the $\acute{z}$-axis is extending along the plate's width. Let the magnetic field $\vec{B}=\left(0,B_0,0\right)$ be oriented parallel to the y-axis and $\vec{q}=(u',0,0)$ be the fluid velocity. Figure 1 outlines the physical structure of our model.

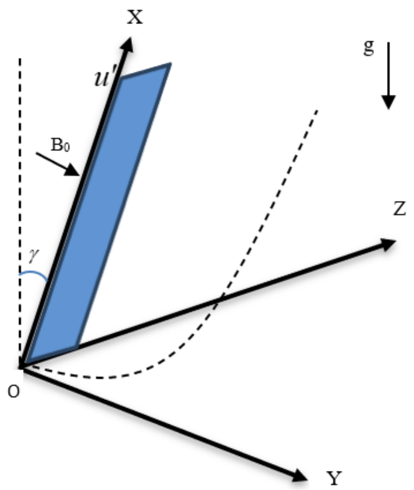

Figure 1. Geometric configuration.

Equation (4) becomes:

$$\rho\frac{\partial u'}{\partial \bar{t}}\hat{i}=\mu\frac{\partial^2 u'}{\partial y'^2}\hat{i}-\rho g\cos\gamma\hat{i}-\left(\frac{\partial p}{\partial x'}\hat{i}+\frac{\partial p}{\partial y'}\hat{j}\right)-\sigma B_0^2 u'\hat{i}. \qquad (11)$$

By aligning the coefficients $\hat{i}$, we obtain:

$$\rho\frac{\partial u'}{\partial \bar{t}}=\mu\frac{\partial^2 u'}{\partial y'^2}-\rho g\cos\gamma-\frac{\partial p}{\partial x'}-\sigma B_0^2 u'. \qquad (12)$$

In the fluid domain remote from the plate, Equation (12) reduces to:

$$0 = -\rho_\infty g \cos\gamma - \frac{\partial p}{\partial x'} \tag{13}$$

Using Equations (7) and (13), Equation (12) reduces to:

$$\frac{\partial u'}{\partial \bar{t}} = \nu \frac{\partial^2 u'}{\partial y'^2} - g\beta\left(T - T_\infty\right)\cos\gamma + g\beta^*\left(C - C_\infty\right)\cos\gamma - \frac{\sigma B_0^2 u'}{\rho}. \tag{14}$$

Equation (10) becomes:

$$\rho C_p \frac{\partial T}{\partial \bar{t}} = \kappa \frac{\partial^2 T}{\partial y'^2} + \bar{J}\left(T_\infty - T\right) + \frac{16\sigma^* T_\infty^3}{3\kappa^*}\frac{\partial^2 T}{\partial y'^2}. \tag{15}$$

Equation (6) becomes:

$$\frac{\partial C}{\partial \bar{t}} = D_M \frac{\partial^2 C}{\partial y'^2} + \bar{K}\left(C_\infty - C\right) + \frac{D_M K_T}{T_m}\frac{\partial^2 T}{\partial y'^2}. \tag{16}$$

The introductory boundary restrictions (Gohain *et al.* [23]):

$$\left.\begin{array}{l} \forall\ y' \ge 0 : u' = 0, T = T_\infty, C = C_\infty, \text{ for } \bar{t} \le 0, \\ \text{At } y' = 0 : \begin{cases} u' = \dfrac{U_0 \bar{t}}{t_0}, T = T_\infty + \dfrac{T_w - T_\infty}{t_0}\bar{t}, C = C_\infty + \dfrac{C_w - C_\infty}{t_0}\bar{t}, \text{ for } 0 < \bar{t} \le t_0, \\ u' = U_0, T = T_w, C = C_w, \ \forall\ \bar{t} > t_0 \end{cases} \\ \text{As } y' \to \infty : u' \to 0, T \to T_\infty, C \to C_\infty \ \ \forall\ \bar{t} > 0. \end{array}\right\} \tag{17}$$

Establishing the non-dimensional parameters as:

$$u = \frac{u'}{U_0},\ y = \frac{y'}{U_0 t_0},\ M = \frac{\sigma B_0^2 \nu}{\rho U_0^2},\ \text{Gr} = \frac{\nu g\beta\left(T_w - T_\infty\right)}{U_0^3},\ \text{Gm} = \frac{\nu g\beta^*\left(C_w - C_\infty\right)}{U_0^3},\ \theta = \frac{T - T_\infty}{T_w - T_\infty},$$

$$\phi = \frac{C - C_\infty}{C_w - C_\infty},\ \Pr = \frac{\mu C_P}{\kappa},\ \text{Sc} = \frac{\nu}{D_M},\ Ra = \frac{U_0^2}{\nu}t_0,\ N = \frac{\kappa\kappa^*}{4\sigma^* T_\infty^3},\ K = \bar{K}t_0,\ \text{Sr} = \frac{D_M K_T\left(T_w - T_\infty\right)}{\nu T_m\left(C_w - C_\infty\right)},$$

$$t = \frac{\bar{t}}{t_0},\ J = \frac{\bar{J}t_0}{\rho C_p}.$$

Adopting the above unitless parameters, equations (14), (15), and (16) becomes:

$$\frac{\partial u}{\partial t} = \frac{1}{Ra}\frac{\partial^2 u}{\partial y^2} + \text{Gr}Ra\theta\cos\gamma + \text{Gm}Ra\phi\cos\gamma - MuRa, \tag{18}$$

$$\frac{\partial \theta}{\partial t} = \frac{\Gamma}{\Pr Ra}\frac{\partial^2 \theta}{\partial y^2} - J\theta, \tag{19}$$

$$\frac{\partial \phi}{\partial t} = \frac{1}{\text{Sc}Ra}\frac{\partial^2 \phi}{\partial y^2} - K\phi + \frac{\text{Sr}}{Ra}\frac{\partial^2 \theta}{\partial y^2}. \tag{20}$$

where $\Gamma = 1 + \dfrac{4}{3N}$.

In a dimensionless layout, the introductory boundary restrictions are:

$$\left.\begin{array}{l} \forall\ y \ge 0 : u = \theta = \phi = 0\ ;\ \text{for } t \le 0, \\ \text{At } y = 0 : \begin{cases} u = \theta = \phi = t\ ;\ \text{for } 0 < t \le 1, \\ u = \theta = \phi = 1\ ;\ \forall\ t > 1, \end{cases} \\ \text{As } y \to \infty : u \to 0, \theta \to 0, \phi \to 0\ ;\ \forall\ t > 0. \end{array}\right\} \tag{21}$$

4. Solution Methodology

Solving the issue with precision necessitates using the Laplace transform technique on both the equations (18)-(20) and restrictions (21), yielding the following solutions:

$$\frac{d^2\bar{u}}{dy^2} - Ra(s+M)\bar{u} = -Ra^2\mathrm{Gr}\bar{\theta}\cos\gamma - Ra^2\mathrm{Gm}\bar{\phi}\cos\gamma, \tag{22}$$

$$\frac{d^2\bar{\theta}}{dy^2} - \Lambda\left(J+s\right)\bar{\theta} = 0, \tag{23}$$

$$\frac{d^2\bar{\phi}}{dy^2} - Ra\mathrm{Sc}\left(s+K\right)\bar{\phi} = -\mathrm{SrSc}\frac{d^2\bar{\theta}}{dy^2}. \tag{24}$$

Where $\Lambda = \frac{\mathrm{Pr}Ra}{\Gamma}$.

Subject to the restrictions:

$$\left.\begin{array}{l} \text{At } y=0: \bar{u}=\bar{\theta}=\bar{\phi}=S_0, \\ \text{As } y\to\infty: \bar{u}\to 0, \bar{\theta}\to 0, \bar{\phi}\to 0. \end{array}\right\} \tag{25}$$

Where $S_0 = \frac{1}{s^2}\left(1-e^{-s}\right)$.

Solutions of the equations (22)-(24) under the restrictions (25) are as follows:

$$\bar{\theta} = S_0 e^{-\sqrt{\Lambda(s+J)}y}, \tag{26}$$

$$\bar{\phi} = \left(S_0 + AS_1\right)e^{-\sqrt{Ra\mathrm{Sc}(s+K)}y} - AS_1 e^{-\sqrt{\Lambda(s+J)}y}, \tag{27}$$

$$\bar{u} = \left(S_0 - S_5 - N_2S_3\right)e^{-\sqrt{Ra(s+M)}y} + S_5e^{-\sqrt{\Lambda(s+J)}y} + N_2S_3e^{-\sqrt{Ra\mathrm{Sc}(s+K)}y}. \tag{28}$$

Upon performing the Laplace inverse transformation on Equations (26)-(28), the resulting expressions for dimensionless energy θ, concentration ϕ, and velocity u are obtained as follows:

$$\theta = \xi_1, \tag{29}$$

$$\phi = \xi_2 + A\xi_4 - A\xi_6, \tag{30}$$

$$u = u_1 + u_2 + u_3. \tag{31}$$

4.1. Skin friction.

The momentum transport rate is given by:

$$\tau = -\left.\frac{\partial u}{\partial y}\right]_{y=0} = -\left(\tau_1+\tau_2+\tau_3\right). \tag{32}$$

4.2. Nusselt number.

$$\mathrm{Nu} = -\left.\frac{\partial \theta}{\partial y}\right]_{y=0} = -\Pi_1. \tag{33}$$

4.3. Sherwood number.

$$\mathrm{Sh} = -\left.\frac{\partial \phi}{\partial y}\right]_{y=0} = -\left(\Pi_2 + A\Pi_4 - A\Pi_6\right). \tag{34}$$

5. Results and Discussion

To understand the physical mechanisms governing the current issue, a parametric evaluation has been executed, and the computed outcomes for dimensionless velocity, concentration, temperature, the coefficient of viscous drag, Sherwood, and Nusselt numbers are illustrated in the accompanying graphs. While conducting this investigation, the Prandtl number Pr=0.71 and Schmidt number Sc=0.60, representing air as solvent and water-vapor as solute, respectively, have been consistently kept fixed.

The influences of Soret number Sr, magnetic parameter *M*, ramped parameter *Ra*, chemical reaction parameter *K*, angle of inclination γ, solutal Grashof number Gm, thermal Grashof number Gr, and radiation parameter *N* on the dimensionless velocity are illustrated in Figures 2-9. Figure 2 depicts that the fluid velocity u rises as a result of increasing Sr for both t<1 and t>1 conditions. This suggests that a rise in Sr enhances molecular diffusivity, boosting the fluid velocity.

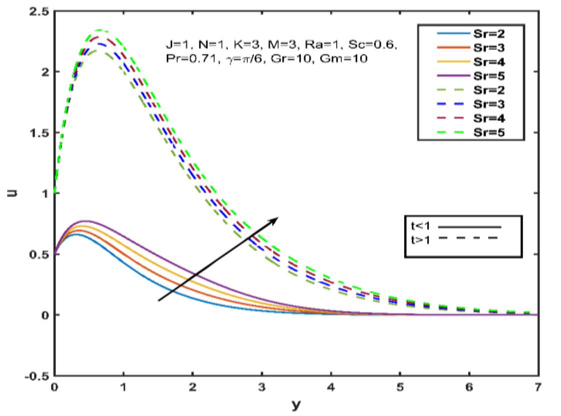

Figure 2. *u* influenced by Sr.

In both t<1 and t>1 scenarios, an increase in *M* leads to a reduction in fluid velocity, as shown in Figure 3. The decrease in velocity is attributed to the transverse magnetic fields, which generate a resistive force (Lorentz force) that counteracts and impedes the flow.

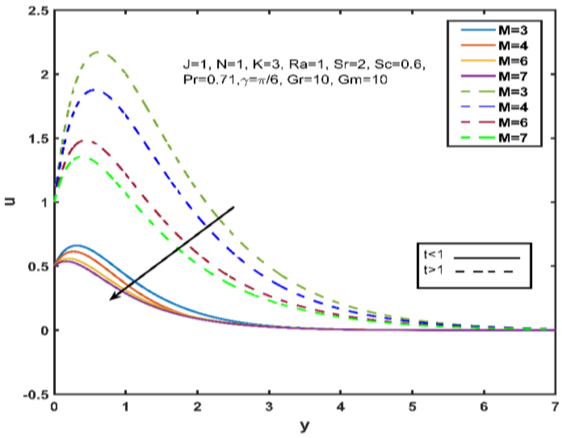

Figure 3. *u* influenced by *M*.

According to Figure 4, in both t<1 and t>1 cases, the velocity profile initially rises near the plate with the increasing ramped parameter, followed by a trend reversal after a critical point.

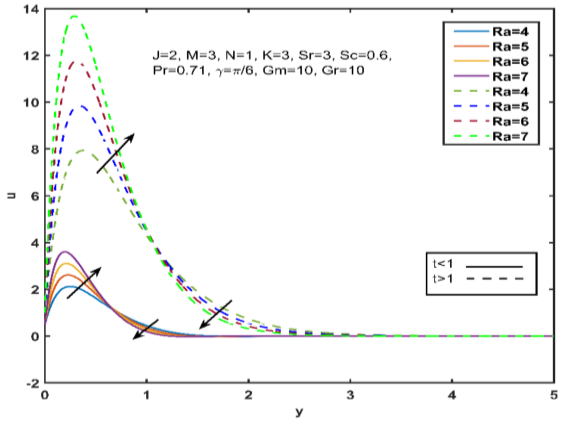

Figure 4. *u* influenced by *Ra*.

Figure 5 highlights that the fluid velocity drops as the value of *K* upsurges for both conditions of t. The advancement in the chemical reaction parameter decreases the concentration field, thereby reducing the buoyancy effects driven by the concentration gradient, causing a drop in velocity.

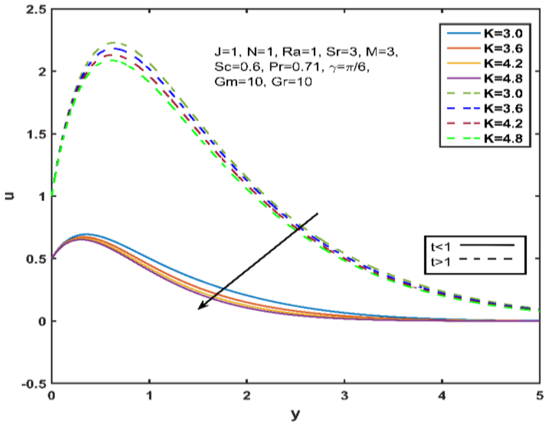

Figure 5. *u* influenced by *K*.

Figure 6 indicates that as the angle of inclination grows, the velocity decreases for both t<1 and t>1 scenarios.

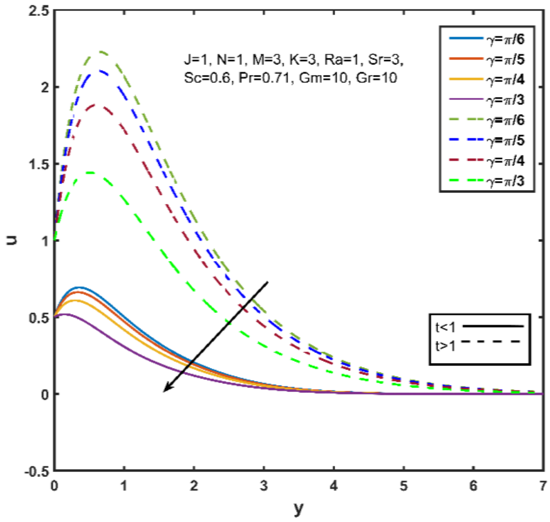

Figure 6. *u* influenced by γ .

It is clear that in both t<1 and t>1 conditions, the velocity accelerates with the expansion of Gm, as displayed in Figure 7. This outcome can be ascribed to either enhanced buoyancy force or diminished fluid viscosity.

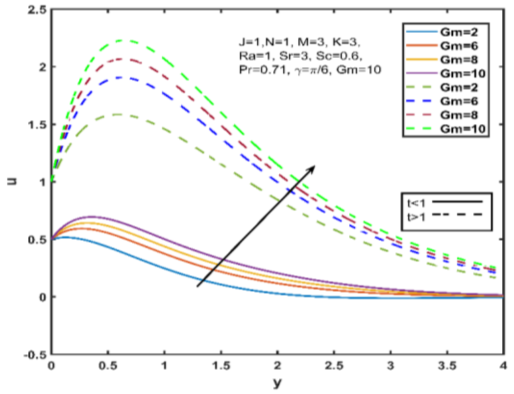

Figure 7. *u* influenced by Gm.

It is visible from Figure 8 that when t<1, the velocity increases as the value of Gr climbs, but after reaching a critical point, the behavior reverses. Conversely, when t>1, the fluid velocity increases for *Gr*.

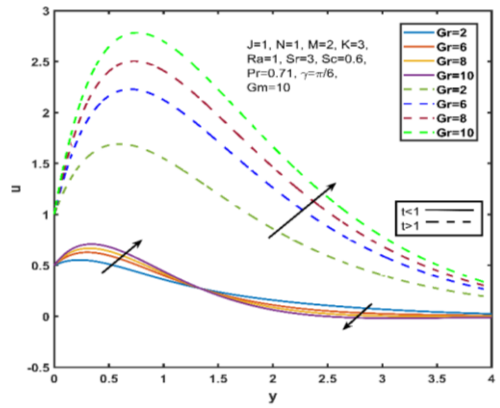

Figure 8. *u* influenced by Gr.

In the case of t<1, there is an increment in fluid velocity as the value of *N* increases. However, for t>1, we observe a contrasting behavior in velocity, as reflected in Figure 9.

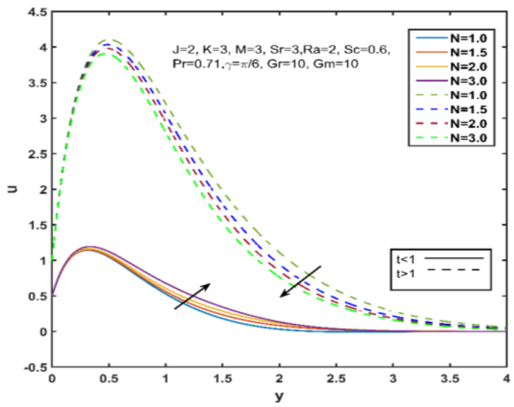

Figure 9. *u* influenced by *N*.

Figures 10-12 present the configuration of the temperature profiles for heat sink parameter *J*, radiation parameter *N*, and ramped parameter *Ra*. The pattern observed in the figures is unaffected by whether the plate is in an isothermal (t>1) or in a ramped state (t<1). Figure 10 displays that the temperature reduces as the value of *J* upsurges. This behavior is attributable to the natural tendency for the temperature to drop when energy is absorbed by the sink.

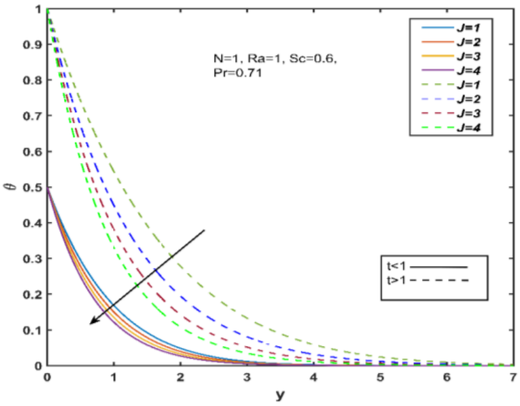

Figure 10. θ influenced by *J*.

Figure 11 depicts how a surge in radiation parameters leads to a comprehensive decline in temperature profile. Radiation is known to decrease temperature in practical systems. This result aligns with the scientific understanding that radiation leads to a reduced temperature profile.

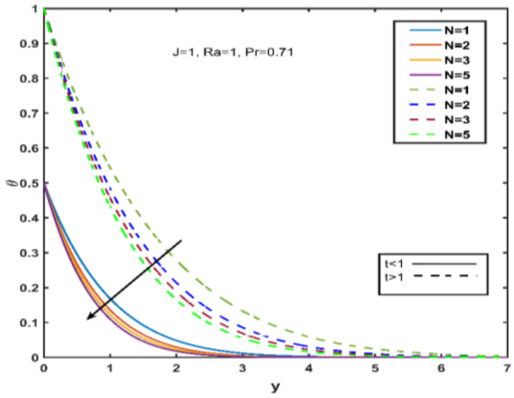

Figure 11. θ influenced by *N*.

The intensification of *Ra* declines the fluid temperature, as demonstrated in Figure 12. A rise in *Ra* suggests a drop in kinematic viscosity, as lower fluid friction leads to a decline in temperature. This observation is consistent with the principle that greater friction leads to higher fluid temperatures.

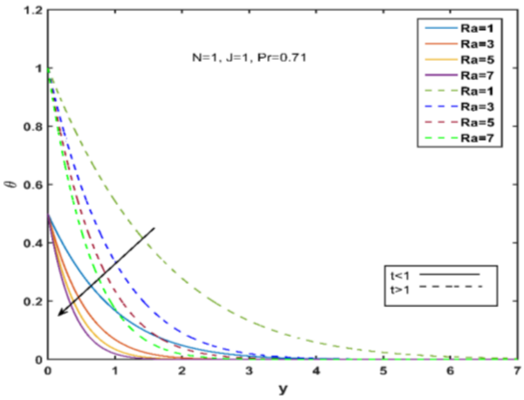

Figure 12. θ influenced by *Ra*.

The variations in the concentration profile under the impacts of thermal diffusion Sr, ramped parameter *Ra*, and chemical reaction parameter *K* are plotted in Figures 13-15. A detailed look at the figures shows that the flow patterns do not differ between t>1 and t<1 conditions. Figure 13 shows that the concentration profile increases with an improved Soret number. A higher Soret number reflects a more pronounced temperature gradient compared to the composition gradient.

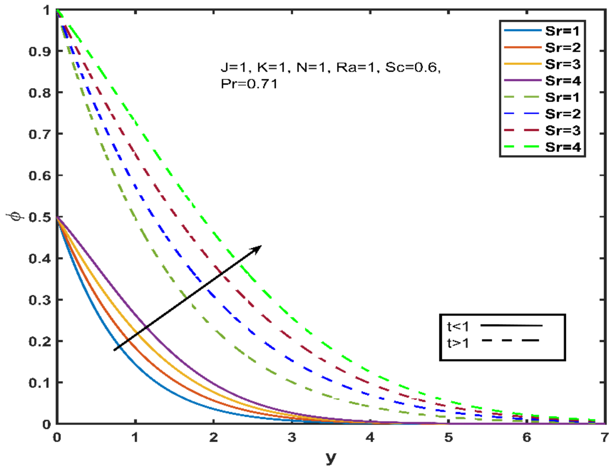

Figure 13. ϕ influenced by Sr.

As a result, this heightened temperature gradient causes an elevation in fluid concentration. Figure 14 reveals a decline in the concentration profile as the ramped parameter *Ra* escalates.

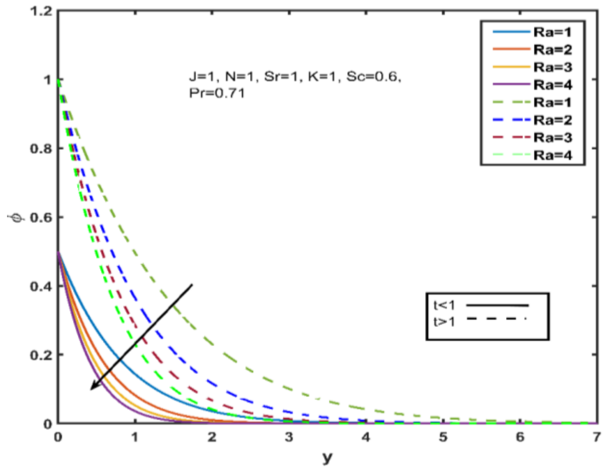

Figure 14. ϕ influenced by *Ra*.

The heightened chemical reaction parameter *K* diminishes the fluid concentration, as shown in Figure 15. The intensification of the chemical reaction causes the concentration boundary layer to thin, thereby reducing the fluid concentration.

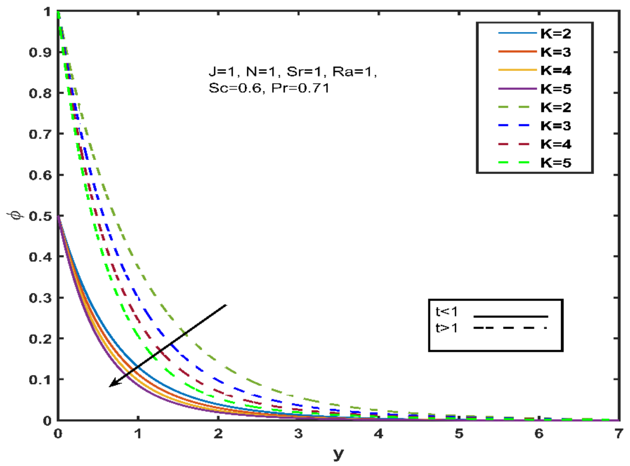

Figure 15. ϕ influenced by *K*.

Figures 16-19 exhibit the behaviors of the skin friction coefficient under the influences of ramped parameter *Ra*, Soret number Sr, angle of inclination γ, and chemical reaction parameter *K*. It is noticeable from Figures 16 and 17 that the viscous drag increases as the values of *Ra* and Sr increases, however, for rising value of γ declines the drag force, as reflected in figure 18. It is apparent from Figures 16 and 17 that the viscous drag lessens as the parameters *Ra* and Sr increase.

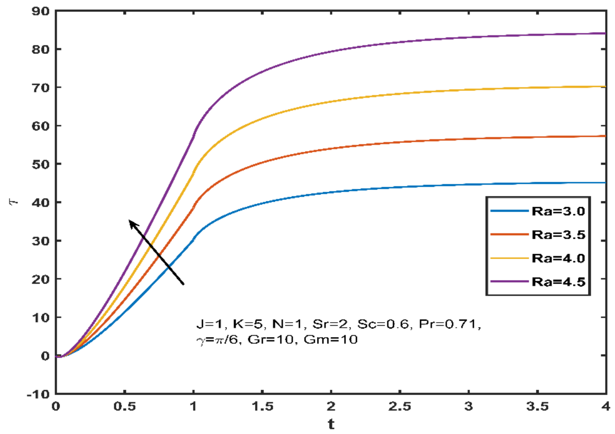

Figure 16. τ influenced by *Ra*.

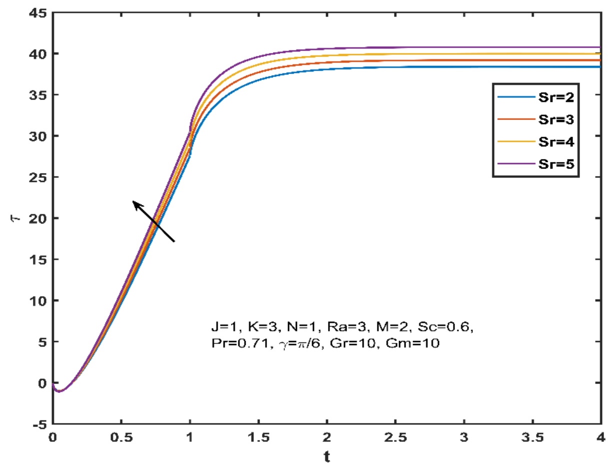

Figure 17. τ influenced by Sr.

However, Figure 18 highlights that a higher γ causes a reduction in drag force. Figure 19 illustrates that as *K* improves, skin friction increases until a critical point is reached, after which a downward trend is monitored.

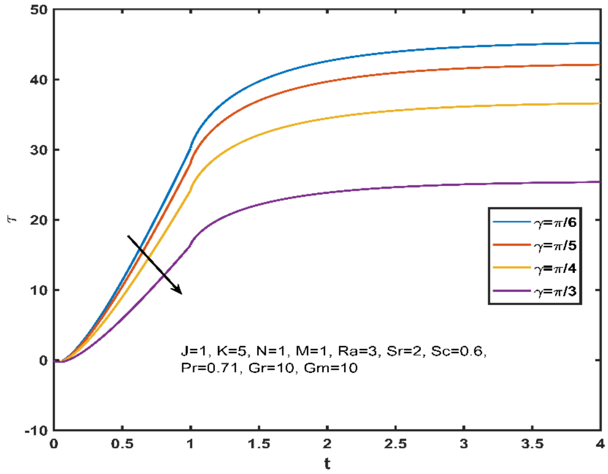

Figure 18. τ influenced by γ.

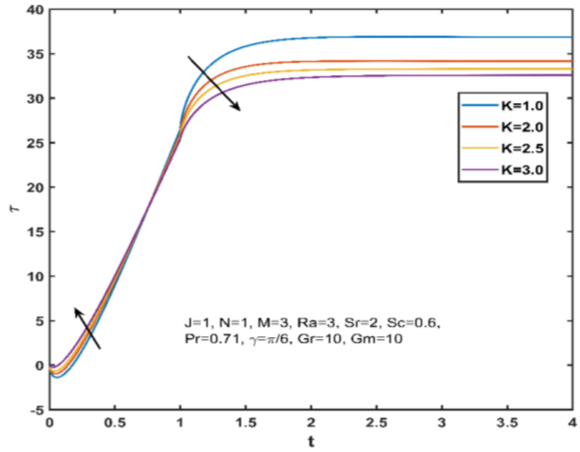

Figure 19. τ influenced by *K*.

The Nusselt number for various values of ramped parameter *Ra*, radiation parameter *N*, and heat sink parameter *J* are illustrated in Figures 20-22. It is seen that the heat transfer rate increases with the rising values of *Ra*, *N*, and *J*. This can be elucidated by the observation that convection facilitates heat transfer more efficiently than conduction, resulting in an elevated Nusselt number as the values of *Ra*, *N*, and *J* increase.

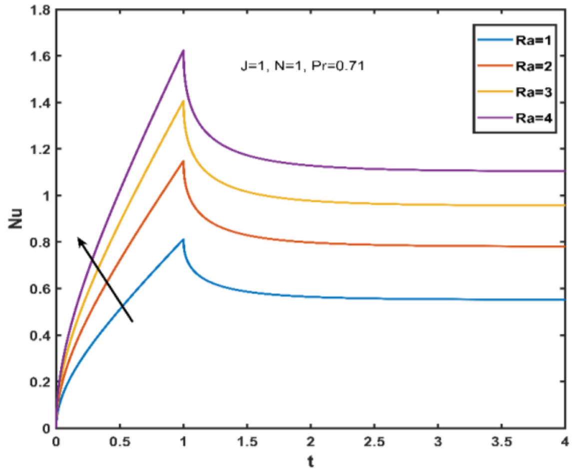

Figure 20. Nu influenced by *Ra*.

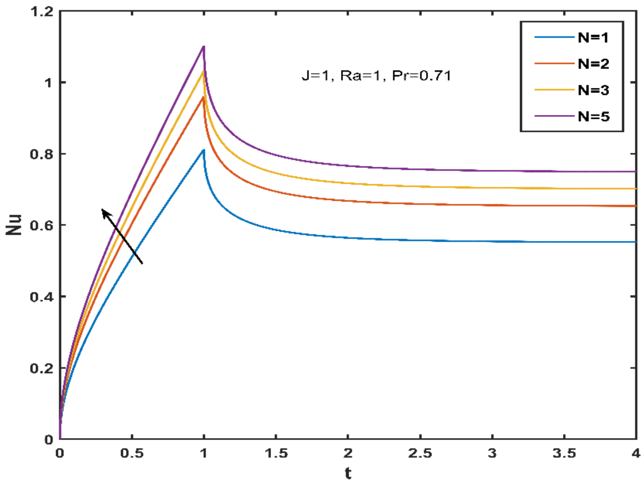

Figure 21. Nu influenced by *N*.

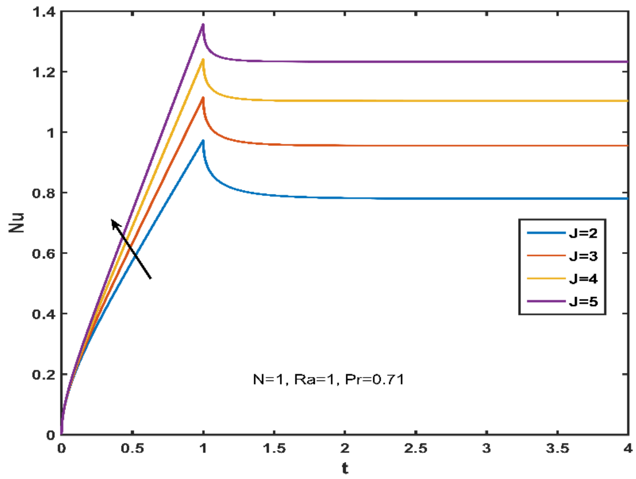

Figure 22. Nu influenced by *J*.

The significances of ramped parameter *Ra*, chemical reaction parameter *K*, and Soret number Sr on mass transfer rate are presented in Figures 23-25. Figures 23 and 24 show that the mass transport rate increases with the intensification of both *Ra* and *K*. This can be attributed to the fact that convection accelerates mass transfer more effectively than diffusion, which in turn results in a higher Sherwood number with increasing *Ra* and *K* values. In contrast, Figure 25 demonstrates that the amplification of the Soret effect drastically decreases the Sherwood number. This is because diffusion promotes mass transfer more rapidly than convection, causing the Sherwood number to diminish with increasing Sr.

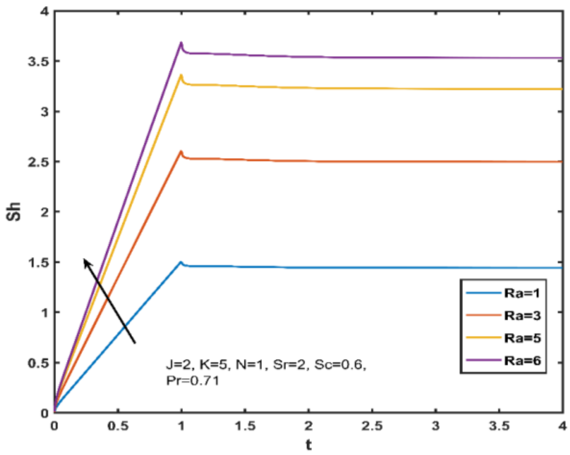

Figure 23. Sh influenced by *Ra*.

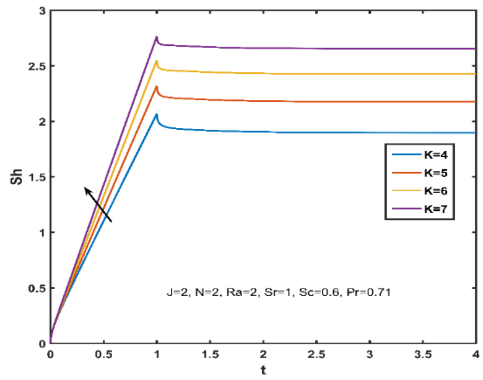

Figure 24. Sh influenced by *K*.

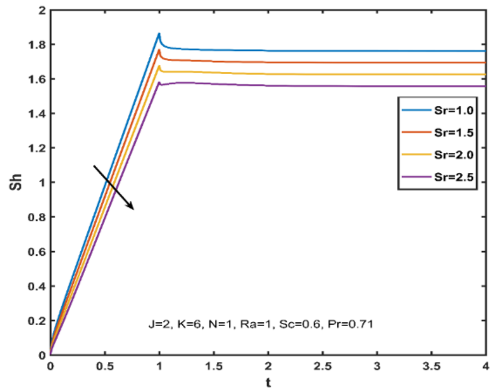

Figure 25. Sh influenced by Sr.

5.1. Comparison and validation of results.

A particular outcome from the present investigation is compared with the study of Reddy *et al*. [33] to verify the consistency of our findings. The variation of the concentration field under the influence of Schmidt number is presented in Figure 26. Figure 26 is compared with Figure 14 of Reddy *et al*. [33]. Figure 26 illustrates that an increasing Sc value enhances the concentration profile, consistent with the observation made in Figure 14 by Reddy *et al*. [33]. Additionally, the authors computed the numerical values of the Sherwood number for the current analysis and performed a comparison with the findings of Reddy *et al*. [33], which is demonstrated in Table 1. From the numerical data of the two models, it is noted that a rise in the chemical reaction parameter leads to an improved rate of mass transfer. These comparisons indicate a high level of agreement between the numerical and graphical solutions, which supports the accuracy and validity of the findings obtained using the current method.

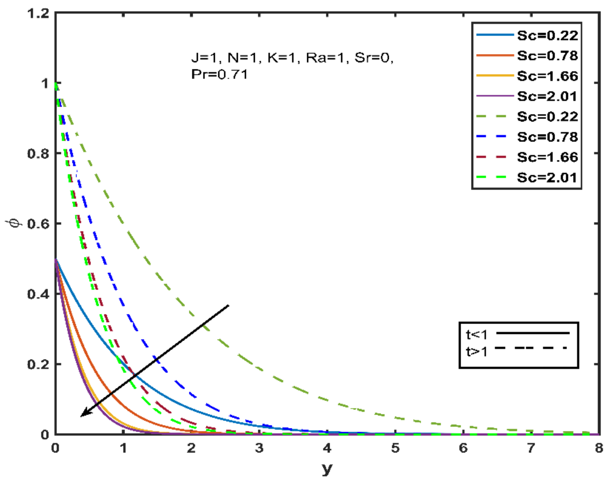

Figure 26. ϕ influenced by Sc.

Table 1. Sherwood number when Pr=0.71, *N*=1, *J*=1, *K*=1, Sc=0.22.

K	Sh (when t=0.5)	
	Work by Reddy *et al.* [34]	Present work with Sr=0, *Ra*=1.
0.2	0.173947	0.3866
2	0.327404	0.4881
5	0.498402	0.6287

6. Conclusions

This analysis primarily concentrates on the hydromagnetic-free convective flow with the Soret effect, thermal radiation, heat absorption, and chemical reaction when ramped conditions are implemented simultaneously. The significant outcomes from our study are summarized as follows: In the case of isothermal conditions, the amplitude of the velocity, concentration, and temperature fields appears higher compared to that under ramped conditions; The fluid velocity slows down with rising magnetic and chemical reaction parameters but speeds up with an increasing Soret number; Both concentration and temperature profiles declined drastically as the ramped parameter increased; The amplification of the heat sink and radiation parameters enhances the heat transport rate; The drag force is amplified due to the thermal diffusion effect. Meanwhile, the mass transport rate experiences the opposite effect; The momentum transfer rate rises in response to increasing chemical reaction parameters, but after reaching a critical point, a contrasting trend is reflected.

Our study ignored the effects of porous media, inclined magnetic fluid, Joule heating, and frictional heating. Therefore, researchers can extend this work by incorporating these aforementioned effects.

Appendix

$$S_1=\frac{S_0\left(s+J\right)}{s+a},\ S_2=S_0+AS_1,\ S_3=\frac{S_2}{Ra\left(\mathrm{Sc}-1\right)\left(s+c\right)},\ S_4=\frac{AS_1}{\left(\Lambda-Ra\right)\left(s+b\right)},$$

$$S_5=\frac{N_1S_0}{\left(s+b\right)}-S_4N_2,\ A=\frac{\mathrm{SrSc}\Lambda}{\Lambda-Ra\mathrm{Sc}},\ a=\frac{\Lambda J-Ra\mathrm{Sc}K}{\Lambda-Ra\mathrm{Sc}},\ b=\frac{\Lambda J-RaM}{\Lambda-Ra},\ c=\frac{\mathrm{Sc}K-M}{\mathrm{Sc}-1},$$

$$N_1=\frac{-Ra^2\mathrm{Gr}\cos\gamma}{\Lambda-Ra},\ N_2=-Ra^2\mathrm{Gm}\cos\gamma,$$

$$u_1=u_{1,1}+u_{1,2}+u_{1,3},\ u_{1,1}=\xi_7,\ u_{1,2}=\frac{N_2A}{\Lambda-Ra}\Delta\xi_8-N_1\Delta\xi_9,\ u_{1,3}=\xi_{12},\ u_2=\xi_{14}-\xi_{16},\ u_3=\xi_{19},$$

$$\xi_1=\Delta f_1,\ \xi_2=\Delta f_2,\ \xi_3=A_1\psi_1+A_2\psi_2+A_3f_2,\ \xi_4=\Delta\xi_3,\ \xi_5=A_1\psi_3+A_2\psi_4+A_3f_1,\ \xi_6=\Delta\xi_5,$$

$$\xi_7=\Delta f_3,\ \xi_8=A_4\psi_5+A_5\psi_6+A_6\psi_7+A_7f_3,\ \xi_9=A_8\psi_6+A_9\psi_7+A_{10}f_3,\ \xi_{10}=A_{11}\psi_8+A_{12}\psi_7+A_{13}f_3,$$

$$\xi_{11}=A_{14}\psi_5+A_{15}\psi_8+A_{16}\psi_7+A_{17}f_3,\ \xi_{12}=\frac{-N_2}{Ra\left(\mathrm{Sc}-1\right)}\left(\Delta\xi_{10}+A\Delta\xi_{11}\right),\ \xi_{13}=A_8\psi_9+A_9\psi_4+A_{10}f_1,$$

$$\xi_{14}=N_1\Delta\xi_{13},\ \xi_{15}=A_4\psi_3+A_5\psi_9+A_6\psi_4+A_7f_1,\ \xi_{16}=\frac{N_2A}{\Lambda-Ra}\Delta\xi_{15},\ \xi_{17}=A_{11}\psi_{10}+A_{12}\psi_2+A_{13}f_2,$$

$$\xi_{18}=A_{14}\psi_1+A_{15}\psi_{10}+A_{16}\psi_2+A_{17}f_2,\ \xi_{19}=\frac{N_2}{Ra\left(\mathrm{Sc}-1\right)}\left(\Delta\xi_{17}+A\Delta\xi_{18}\right),\ A_1=\frac{J-a}{a^2},\ A_2=-A_1,$$

$$A_3=\frac{J}{a},\ A_4=\frac{J-a}{\left(b-a\right)a^2},\ A_5=\frac{J-b}{\left(a-b\right)b^2},\ A_6=-\left(A_4+A_5\right),\ A_7=\frac{J}{ab},\ A_8=\frac{1}{b^2},\ A_9=-A_8,$$

$A_{10}=\frac{1}{b},\ A_{11}=\frac{1}{c^2},\ A_{12}=-A_{11},\ A_{13}=\frac{1}{c},\ A_{14}=\frac{J-a}{(c-a)a^2},\ A_{15}=\frac{J-c}{(a-c)c^2},\ A_{16}=-(A_{14}+A_{15}),$

$A_{17}=\frac{J}{ac},$

$f_1=f(\Lambda,J,y,t),\ f_2=f(Ra\mathrm{Sc},K,y,t),\ f_3=f(Ra,M,y,t),\ \psi_1=\Psi(Ra\mathrm{Sc},K,-a,y,t),$
$\psi_2=\psi(Ra\mathrm{Sc},K,y,t),\ \psi_3=\Psi(\Lambda,J,-a,y,t),\ \psi_4=\psi(\Lambda,J,y,t),\ \psi_5=\Psi(Ra,M,-a,y,t),$
$\psi_6=\Psi(Ra,M,-b,y,t),\ \psi_7=\psi(Ra,M,y,t),\ \psi_8=\Psi(Ra,M,-c,y,t),$
$\psi_9=\Psi(\Lambda,J,-b,y,t),\ \psi_{10}=\Psi(Ra\mathrm{Sc},K,-c,y,t),\ \tau_1=\tau_{1,1}+\tau_{1,2}+\tau_{1,3},\ \tau_{1,1}=\Pi_7,$
$\tau_{1,2}=\frac{N_2A}{\Lambda-Ra}\Delta\Pi_8-N_1\Delta\Pi_9,\ \tau_{1,3}=\Pi_{12},\ \tau_2=\Pi_{14}-\Pi_{16},\ \tau_3=\Pi_{19},\ \Pi_1=\Delta\Phi_1,\ \Pi_2=\Delta\Phi_2,$
$\Pi_3=A_1\Omega_1+A_2\Omega_2+A_3\Phi_2,\ \Pi_4=\Delta\Pi_3,\ \Pi_5=A_1\Omega_3+A_2\Omega_4+A_3\Phi_1,\ \Pi_6=\Delta\Pi_5,\ \Pi_7=\Delta\Phi_3,$
$\Pi_8=A_4\Omega_5+A_5\Omega_6+A_6\Omega_7+A_7\Phi_3,\ \Pi_9=A_8\Omega_6+A_9\Omega_7+A_{10}\Phi_3,\ \Pi_{10}=A_{11}\Omega_8+A_{12}\Omega_7+A_{13}\Phi_3,$
$\Pi_{11}=A_{14}\Omega_5+A_{15}\Omega_8+A_{16}\Omega_7+A_{17}\Phi_3,\ \Pi_{12}=\frac{-N_2}{Ra(\mathrm{Sc}-1)}(\Delta\Pi_{10}+A\Delta\Pi_{11}),$
$\Pi_{13}=A_8\Omega_9+A_9\Omega_4+A_{10}\Phi_1,\ \Pi_{14}=N_1\Delta\Pi_{13},\ \Pi_{15}=A_4\Omega_3+A_5\Omega_9+A_6\Omega_4+A_7\Phi_1,$
$\Pi_{16}=\frac{N_2A}{\Lambda-Ra}\Delta\Pi_{15},\ \Pi_{17}=A_{11}\Omega_{10}+A_{12}\Omega_2+A_{13}\Phi_2,\ \Pi_{18}=A_{14}\Omega_1+A_{15}\Omega_{10}+A_{16}\Omega_2+A_{17}\Phi_2,$
$\Pi_{19}=\frac{N_2}{Ra(\mathrm{Sc}-1)}(\Delta\Pi_{17}+A\Delta\Pi_{18}),\ \Phi_1=\Phi(\Lambda,J,y,t),\ \Phi_2=\Phi(Ra\mathrm{Sc},K,y,t),$
$\Phi_3=\Phi(Ra,M,y,t),\ \Omega_1=Z(Ra\mathrm{Sc},K,-a,y,t),\ \Omega_2=\Omega(Ra\mathrm{Sc},K,y,t),$
$\Omega_3=Z(\Lambda,J,-a,y,t),\ \Omega_4=\Omega(\Lambda,J,y,t),\ \Omega_5=Z(Ra,M,-a,y,t),\ \Omega_6=Z(Ra,M,-b,y,t),$
$\Omega_7=\Omega(Ra,M,y,t),\ \Omega_8=Z(Ra,M,-c,y,t),\ \Omega_9=Z(\Lambda,J,-b,y,t),$
$\Omega_{10}=Z(Ra\mathrm{Sc},K,-c,y,t),\ \Psi(\xi,\eta,\zeta,y,t)=e^{\zeta t}\psi(\xi,\eta+\zeta,y,t),$
$Z(\xi,\eta,\zeta,t)=e^{\zeta t}\Omega(\xi,\eta+\zeta,t),\ \psi=\psi(x,y,z,...,t)\Rightarrow\bar{\psi}=\psi(x,y,z,...,t-1)H(t-1),$
$\Delta S_m=S_m-\bar{S}_m,$

$$\Omega(\xi,\ell,t)=-\left[\sqrt{\frac{\xi}{\pi t}}e^{-\ell t}+\sqrt{\xi\ell}\,erf\left(\sqrt{\ell t}\right)\right],$$

$$\Phi(\xi,\ell,t)=-\left[\sqrt{\frac{\xi}{4\ell}}erf\left(\sqrt{\ell t}\right)+t\sqrt{\xi\ell}\,erf\left(\sqrt{\ell t}\right)+\sqrt{\frac{\xi t}{\pi}}e^{-\ell t}\right].$$

$$f(\xi,\ \ell,\ y,\ t)\ =\ \left(\frac{t}{2}+\frac{y}{4}\sqrt{\frac{\xi}{\ell}}\right)e^{\sqrt{\xi\ell}y}erfc\left(\frac{y}{2}\sqrt{\frac{\xi}{t}}+\sqrt{\ell t}\right)+\left(\frac{t}{2}-\frac{y}{4}\sqrt{\frac{\xi}{\ell}}\right)e^{-\sqrt{\xi\ell}y}erfc\left(\frac{y}{2}\sqrt{\frac{\xi}{t}}-\sqrt{\ell t}\right),$$

$$\psi(\xi,\ \ell,\ y,\ t)\ =\ \frac{1}{2}\left[e^{\sqrt{\xi\ell}y}erfc\left(\frac{y}{2}\sqrt{\frac{\xi}{t}}+\sqrt{\ell t}\right)+e^{-\sqrt{\xi\ell}y}erfc\left(\frac{y}{2}\sqrt{\frac{\xi}{t}}-\sqrt{\ell t}\right)\right].$$

$$H(t-1)=\begin{cases}0, & t<1,\\ \frac{1}{2}, & t=0,\\ 1, & t>1.\end{cases}$$

Funding

This research received no external funding.

Acknowledgments

The authors would like to thank the honorable reviewers and the editorial board.

Conflicts of Interest

The authors declare no conflict of interest.

References

1. Veera Krishna, M. Hall and ion slip effects on MHD free convective rotating flow bounded by the semi-infinite vertical porous surface. *Heat Transfer* **2020**, *49*, 1920-1938, https://doi.org/10.1002/htj.21700.
2. Kataria, H.R.; Patel, H.R. Effect of thermo-diffusion and parabolic motion on MHD Second grade fluid flow with ramped wall temperature and ramped surface concentration. *Alexandria Engineering Journal* **2018**, *57*, 73-85, https://doi.org/10.1016/j.aej.2016.11.014.
3. Roy, N.C. MHD natural convection of a hybrid nanofluid in an enclosure with multiple heat sources. *Alexandria Engineering Journal* **2022**, *61*, 1679-94, https://doi.org/10.1016/j.aej.2021.06.076.
4. Kumar, M.A.; Reddy, Y.D.; Rao, V.S.; Goud, B.S. Thermal radiation impact on MHD heat transfer natural convective nano fluid flow over an impulsively started vertical plate. *Case studies in thermal engineering* **2021**, *24*, 100826, https://doi.org/10.1016/j.csite.2020.100826.
5. Anwar, T.; Kumam, P.; Shah, Z.; Watthayu, W.; Thounthong, P. Unsteady radiative natural convective MHD nanofluid flow past a porous moving vertical plate with heat source/sink. *Molecules* **2020**, *25*, 854, https://doi.org/10.3390/molecules25040854.
6. Karmakar, P.; Das, S.; Mahato, N.; Ali, A.; Jana, R.N. Dynamics prediction using an artificial neural network for a weakly conductive ionized fluid streamed over a vibrating electromagnetic plate. *The European Physical Journal Plus* **2024**, *139*, 407, https://doi.org/10.1140/epjp/s13360-024-05197-w.
7. Dowerah, R.D.; Ahmed, N.; Deka, H. Radiation absorption effect on MHD natural convective flow past an impulsively started infinite vertical plate with chemical reaction and thermal radiation. *Heat Transfer* **2024**, *53*, 2689-2711, https://doi.org/10.1002/htj.23057.
8. Das, S.; Mahato, N.; Ali, A.; Jana, R.N. Dynamics pattern of a radioactive rGO-magnetite-water flowed by a vibrated Riga plate sensor with ramped temperature and concentration. *Chemical Engineering Journal Advances* **2023**, *15*, 100517, https://doi.org/10.1016/j.ceja.2023.100517.
9. Sedki, A.M. Effect of thermal radiation and chemical reaction on MHD mixed convective heat and mass transfer in nanofluid flow due to nonlinear stretching surface through porous medium. *Results in Materials* **2022**, *16*, 100334, https://doi.org/10.1016/j.rinma.2022.100334.
10. Verma, K. MHD flow in porous medium through an exponentially stretching sheet with surface heat and mass flux under the impact of chemical reaction. *Latin American Applied Research-An international journal* **2023**, *53*, 295-302, https://doi.org/10.52292/j.laar.2023.1194.
11. Saikia, D.J.; Ahmed, N. Chemical reaction and radiation impact on unsteady free convective flow through a porous medium past an infinite oscillatory vertical plate. *ZAMM-Journal of Applied Mathematics and Mechanics/Zeitschrift für Angewandte Mathematik und Mechanik* **2024**, *104*, e202200579, https://doi.org/10.1002/zamm.202200579.
12. Kataria, H.R.; Patel, H.R. Radiation and chemical reaction effects on MHD Casson fluid flow past an oscillating vertical plate embedded in porous medium. *Alexandria Engineering Journal* **2016**, *55*, 583-595, https://doi.org/10.1016/j.aej.2016.01.019.

13. Ibrahim, S.M.; Suneetha, K. Effects of thermal diffusion and chemical reaction on MHD transient free convection flow past a porous vertical plate with radiation, temperature gradient dependent heat source in slip flow regime. *Journal of Computational and Applied Research in Mechanical Engineering* **2016**, *5*, 83-95.
14. Ali, A.; Sarkar, S.; Das, S.; Jana, R.N. A report on entropy generation and Arrhenius kinetics in magneto-bioconvective flow of Cross nanofluid over a cylinder with wall slip. *International Journal of Ambient Energy* **2022**, *15*, 1-6, https://doi.org/10.1080/01430750.2022.2031292.
15. Das, S.; Ali, A.; Jana, R.N. Darcian slip flow of rotating magnetoreactive PEG conveying MoS 2 Casson nanofluid with ramped temperature and concentration. *Special Topics & Reviews in Porous Media: An International Journal* **2020**, *11*, 71-102, http://dx.doi.org/10.1615/SpecialTopicsRevPorousMedia.2020030547.
16. Ali, A.; Das, S.; Jana, R.N. Oblique rotational dynamics of chemically reacting tri-hybridized nanofluids over a suddenly moved plate subject to Hall and ion slip currents, Newtonian heating and mass fluxes. *Journal of the Indian Chemical Society* **2023**, *100*, 100983, https://doi.org/10.1016/j.jics.2023.100983.
17. Ali, A.; Banerjee, S.M.; Das, S. Hall and ion slip current's impact on magneto-sodium alginate hybrid nanoliquid past a moving vertical plate with ramped heating, velocity slip and Darcy effects. Multidiscipline Modeling in Materials and Structures **2020**, *17*, 65-101, https://doi.org/10.1108/MMMS-12-2019-0218.
18. Eckert, E.R.G.; Drake, R.M. Analysis of heat and mass transfer. CRC Press, **1986**.
19. Mopuri, O.; Ganteda, C.; Mahanta, B.; Lorenzini, G. MHD heat and mass transfer steady flow of a convective fluid through a porous plate in the presence of multiple parameters. *Journal of Advanced Research in Fluid Mechanics and Thermal Sciences* **2022**, *89*, 56-75, https://doi.org/10.37934/arfmts.89.2.5675.
20. Raghunath; K. Study of heat and mass transfer of an unsteady magnetohydrodynamic (MHD) nanofluid flow past a vertical porous plate in the presence of chemical reaction, radiation and Soret effects. *Journal of Nanofluids* **2023**, *12*, 767-776, https://doi.org/10.1166/jon.2023.1965.
21. Agrawal, A.; Panda, J.P. The Soret effect on MHD flow with Hall current and induced magnetic field. *International Journal of Ambient Energy* **2023**, *44*, 450-462, https://doi.org/10.1080/01430750.2022.2128416.
22. Goud, B.S.; Reddy, Y.D. Chemical reaction and Soret effect on an unsteady MHD heat and mass transfer fluid flow along an infinite vertical plate with radiation and heat absorption. *Journal of the Indian Chemical Society* **2022**, *99*, 100762, https://doi.org/10.1016/j.jics.2022.100762.
23. Gohain, D.; Taid, B.K.; Ahmed, N. Natural convective MHD nanofluid flow past a vertical plate embedded in a porous medium with thermal diffusion and hall current. *ZAMM-Journal of Applied Mathematics and Mechanics/Zeitschrift für Angewandte Mathematik und Mechanik* **2023**, *103*, e202200410, https://doi.org/10.1002/zamm.202200410.
24. Endalew, M.F.; Nayak, A. Thermal radiation and inclined magnetic field effects on MHD flow past a linearly accelerated inclined plate in a porous medium with variable temperature. *Heat Transfer—Asian Research* **2019**, *48*, 42-61, https://doi.org/10.1002/htj.21367.
25. Ullah, M.S.; Tarammim, A.; Uddin, M.J. A study of two dimensional unsteady MHD free convection flow over a vertical plate in the presence of radiation. *Open Journal of Fluid Dynamics* **2021**, *11*, 20-33, https://doi.org/10.4236/ojfd.2021.111002.
26. Das, N.; Sarma, S.; Ahmed, N. Thermal diffusion, and thermal radiation effects on unsteady MHD convective flow past an inclined vertical plate. *Latin American Applied Research-An international journal* **2023**, *53*, 341-348, https://doi.org/10.52292/j.laar.2023.1066.
27. Yedhiri, S.R.; Palaparthi, K.K.; Kodi, R.; Asmat, F. Unsteady MHD rotating mixed convective flow through an infinite vertical plate subject to Joule heating, thermal radiation, Hall current, radiation absorption. *Journal of Thermal Analysis and Calorimetry* **2024**, *149*, 8813–8826, https://doi.org/10.1007/s10973-024-12954-7.
28. Ahmmed, S.F.; Biswas, R.; Afikuzzaman, M. Unsteady magnetohydrodynamic free convection flow of nanofluid through an exponentially accelerated inclined plate embedded in a porous medium with variable thermal conductivity in the presence of radiation. *Journal of Nanofluids* **2018**, *7*, 891-901, https://doi.org/10.1166/jon.2018.1520.
29. Ali, A.; Sarkar, S.; Das, S.; Jana, R.N. Investigation of cattaneo–christov double diffusions theory in bioconvective slip flow of radiated magneto-cross-nanomaterial over stretching cylinder/plate with

activation energy. *International Journal of Applied and Computational Mathematics* **2021**, *7*, 208, https://doi.org/10.1007/s40819-021-01144-w.

30. Patel, H.R. Thermal radiation effects on MHD flow with heat and mass transfer of micropolar fluid between two vertical walls. *International Journal of Ambient Energy* **2021**, *42*, 1281-1296, https://doi.org/10.1080/01430750.2019.1594371.
31. Ali, A.; Das, S.; Jana, R.N. MHD gyrating stream of non-Newtonian modified hybrid nanofluid past a vertical plate with ramped motion, Newtonian heating and Hall currents. *ZAMM-Journal of Applied Mathematics and Mechanics/Zeitschrift für Angewandte Mathematik und Mechanik* **2023**, *103*, e202200080, https://doi.org/10.1002/zamm.202200080.
32. 32.Das, S.; Sarkar, S.; Ali, A.; Nath Jana, R. Exploration of magnetically influenced flow dynamics of a dusty fluid induced by the ramped movement of a thermally active plate. *Archive of Applied Mechanics* **2024**, *94*, 407-433, https://doi.org/10.1007/s00419-023-02531-z.
33. Reddy, Y.D.; Goud, B.S.; Kumar, M.A. Radiation and heat absorption effects on an unsteady MHD boundary layer flow along an accelerated infinite vertical plate with ramped plate temperature in the existence of slip condition. *Partial Differential Equations in Applied Mathematics* **2021**, *4*, 100166, https://doi.org/10.1016/j.padiff.2021.100166.